CANCER GENETICS AND EPIGENETICS

IJC INTERNATIONAL JOURNAL of CANCER

The landscape of genetic aberrations in myxofibrosarcoma

Yasuhide Takeuchi[1,2,3,4] | Kenichi Yoshida[1] | Adriane Halik[5] | Annegret Kunitz[5] | Hiromichi Suzuki[1] | Nobuyuki Kakiuchi[1,2] | Yusuke Shiozawa[1] | Akira Yokoyama[1,6] | Yoshikage Inoue[1,2] | Tomonori Hirano[1,2] | Tetsuichi Yoshizato[1] | Kosuke Aoki[1] | Yoichi Fujii[1,2] | Yasuhito Nannya[1,2] | Hideki Makishima[1,2] | Berit Maria Pfitzner[7] | Lars Bullinger[5,8,9] | Masahiro Hirata[3] | Keita Jinnouchi[3] | Yuichi Shiraishi[10] | Kenichi Chiba[10] | Hiroko Tanaka[11] | Satoru Miyano[11] | Takeshi Okamoto[12] | Hironori Haga[3] | Seishi Ogawa[1,2,13] | Frederik Damm[5,8,9] (ORCID)

[1]Department of Pathology and Tumor Biology, Graduate School of Medicine, Kyoto University, Kyoto

[2]Institute for the Advanced Study of Human Biology (WPI-ASHBi), Kyoto University, Kyoto

[3]Department of Diagnostic Pathology, Kyoto University Hospital, Kyoto, Japan

[4]Japan Society for the Promotion of Science for Young Scientists, Tokyo, Japan

[5]Department of Hematology, Oncology, and Cancer Immunology, Charité-Universitätsmedizin Berlin, Freie Universität Berlin, Humboldt-Universität zu Berlin, Berlin Institute of Health, Berlin, Germany

[6]Department of Therapeutic Oncology, Graduate School of Medicine, Kyoto University, Kyoto, Japan

[7]Charité-Universitätsmedizin Berlin, Institut für Pathologie, Berlin, Germany

[8]German Cancer Consortium (DKTK), Berlin, Germany

[9]German Cancer Research Center (DKFZ), Heidelberg, Germany

[10]Center for Cancer Genomic and Advanced Therapeutics, National Cancer Center, Tokyo, Japan

[11]M&D Data Science Center, Tokyo Medical and Dental University, Tokyo, Japan

[12]Department of Orthopaedic Surgery, Kyoto University Hospital, Kyoto, Japan

[13]Department of Medicine, Centre for Haematology and Regenerative Medicine, Karolinska Institute, Stockholm

Correspondence

Seishi Ogawa, Pathology and Tumor Biology, Kyoto University, Yoshida Konoe cho, Sakyo ku, 606 8501, Kyoto.
Email: sogawa-tky@umin.ac.jp

Frederik Damm, Department of Hematology, Oncology, and Cancer Immunology, Charité-Universitätsmedizin Berlin, Augustenburger Platz 1, 13353 Berlin, Germany.
Email: frederik.damm@charite.de

Funding information

This work was supported by Grant in Aid for

Abstract

Myxofibrosarcoma (MFS) is a rare subtype of sarcoma, whose genetic basis is poorly understood. We analyzed 69 MFS cases using whole-genome (WGS), whole-exome (WES) and/or targeted-sequencing (TS). Newly sequenced genomic data were combined with additional deposited 116 MFS samples. WGS identified a high number of structural variations (SVs) per tumor most frequently affecting the *TP53* and *RB1* loci, 40% of tumors showed a BRCAness-associated mutation signature, and evidence of chromothripsis was found in all cases. Most frequently mutated/copy number altered

genes affected known disease drivers such as *TP53* (56.2%), *CDKN2A/B* (29.7%), *RB1* (27.0%), *ATRX* (19.5%) and *HDLBP* (18.9%). Several previously unappreciated genetic aberrations including *MUC17*, *FLG* and *ZNF780A* were identified in more than 20% of patients. Longitudinal analysis of paired diagnosis and relapse time points revealed a 1.2-fold mutation number increase accompanied with substantial changes in clonal composition over time. Our study highlights the genetic complexity underlying sarcomagenesis of MFS.

KEYWORDS

druggable alterations, genetics, myxofibrosarcoma, whole genome/exome/targeted-capture sequence

What's new?

The genetic basis of myxofibrosarcoma, a rare subtype of sarcoma, remains poorly understood. This large-scale integrated genetic study of 185 myxofibrosarcoma cases reveals ubiquitous genetic complexity, including the common occurrence of chromothripsis accompanied with local hypermutation. The results also highlight mutually exclusive alterations in CDKN2A/B and HDLBP on the one hand, and co-occurrence of mutations in *TP53* and other genes implicated in DNA double-strand break repair on the other hand. Taken together, the findings offer a strong rational for investigating PARP inhibition and/or restoration of normal p53 function as potential treatment avenues for myxofibrosarcoma.

1 | INTRODUCTION

Soft tissue sarcomas (STS) are a diverse group of tumors with remarkable histologic diversity leading to more than 50 recognized subtypes.[1] Identification of subtype-specific translocations, including *SS18-SSX* in synovial sarcoma, *FUS-DDIT3* in myxoid/round cell liposarcoma and *BCOR-CCNB3* in Ewing-like and undifferentiated sarcomas, has revolutionized the diagnostics of sarcoma and has provided new insight into oncogenesis.[2,3] In addition, discovery of activating mutations in *KIT* or *PDGFR* in gastrointestinal stromal tumors[4,5] led to routine application of tyrosine kinase inhibitors for these sarcomas, highlighting the great value of genetics for both diagnostics and targeted treatment approaches. Another group of sarcomas are characterized not only by a recurring, tumor-specific genetic alteration, but also by complex karyotypes that are characteristic of severe genetic and chromosomal instability. Most common among this latter group of STS is myxofibrosarcoma (MFS), which typically occurs in late adult life, peaking in the seventh decade and is mainly encountered in the lower extremities.[1] While originally classified as a myxoid-type malignant fibrous histiocytoma, MFS was reclassified as a distinct entity in the WHO classification of 2002 because of its characteristic biological behavior and clinical features, including an infiltrative growth pattern and a high propensity to local recurrence. Besides frequent complex karyotypes, MFS shares many genetic commonalities with leiomyosarcoma (LMS) and undifferentiated pleomorphic sarcoma (UPS), including recurrent alterations affecting known tumor suppressor genes such as *CDKN2A/B*, *TP53* and *NF1*.[6-8] However, the entire molecular pathogenesis of MFS remains incompletely understood due to limited cohort sizes investigated so far.

Here, we conducted a large-scale integrated genetic study of 185 MFSs, including 69 cases from current study and 116 cases from external data sets[7,9] and identified recurrent driver genes, remarkable complex structural variations and high intratumor heterogeneity in MFS.

2 | MATERIALS AND METHODS

2.1 | Patients and samples

The study cohort comprised 185 cases with MFS: 69 cases from the current study, 17 from TCGA data set and 99 from previous report.[7,9] The number of the samples and analysis were summarized in Figure S1.

In the current study, fresh-frozen tumor and normal tissues/peripheral blood were provided by Charité Universitätsmedizin Berlin (17 cases), and formalin-fixed paraffin-embedded (FFPE) tumor and normal tissues were provided by Charité Universitätsmedizin Berlin (25 cases) and Kyoto University Hospital (27 cases). Clinical information is summarized in Table S1. The diagnosis of 69 cases with MFS from current study was confirmed by pathological review according to the 2020 WHO classification. Similar to a previous report,[7] we diagnosed MFS for pleomorphic spindle cell (or rarely epithelioid-appearing) sarcoma of uncertain/undifferentiated phenotype showing stromal myxoid change that accounted for at least 10% of the total tumor volume, according to WHO and Mentzel et al.[10] Histological grades were evaluated based on the overall pathological features of

the tumors. In two cases with multiregional sampling, tumor specimens were annotated as myxoid or solid based on the pathological features that myxoid areas harbored extracellular myxoid matrix with more than 50% of the area, meanwhile solid areas harbored less than 10%. All tumor samples in the discovery set (n = 44) with paired nontumor DNA were from primary tumors. Among the 17 cases with fresh frozen tumor tissue in the discovery cohort, 5 cases with abundant tumor/normal DNA were further analyzed by WGS. Additional 26 cases without matched nontumor DNA were enrolled to our study, among which one case (UPN056) was later removed because the tumor located in abdominal area, and copy number analysis revealed high amplification in both *MDM2* and *CDK4*, both of which are typical findings of liposarcoma.[11] A total of 69 samples including 44 samples from the discovery cohort and 25 additional samples were analyzed as validation cohort. The patient demographics and tumor characteristics of all cases in our study (n = 69) are summarized in Table S1. On 53 tumor samples with available FFPE tissue, immunohistochemical staining (IHC) for TP53 (DO-7, DAKO) was performed. A positive case was indicated by an H score of 50 to 300 and a negative case by an H score of 0 to 49.[12] Macrodissection of thin-sliced unstained tissues on glass slides was performed on FFPE tumor to ensure sample tumor content. DNA was extracted from FFPE tissue, fresh frozen tissue or fresh peripheral blood using a DNeasy Tissue Kit, a Gentra Puregene Blood Kit or a GeneRead DNA FFPE Kit (all from QIAGEN), according to the manufacturer's protocols, as previously described.[13,14] DNA was quantified using a Qubit Fluorometer (Life Technologies, Carlsbad, California). Sequence data from 17 MFSs from the TCGA dataset[9] and 99 MFSs from a previous report[7] were enrolled to our study.

2.2 | WES, targeted deep sequencing, WGS and confirmatory deep sequencing

For WES, paired tumor (fresh frozen and FFPE tissues) and germline (tumor-free tissue or peripheral blood) samples were collected from all patients. WES libraries were prepared from 100 to 500 ng of genomic DNA and generated using a SureSelect Human All Exon V5 kit/V5 + UTR kit (Agilent Technologies), followed by massively parallel sequencing of enriched exon fragments on a HiSeq 2500 with 125-base pair paired-end mode, as previously described.[13] Following the manufacturers' protocols, libraries from FFPE samples were prepared using a KAPA Hyper Prep Kit (Kapa Biosystems) or a SureSelect Target Enrichment System (Agilent Technologies). The mean coverage of WES was 100.3×, and in average 90.6% of coding regions were analyzed at a depth of more than 20×.

For targeted deep sequencing (TS), tumor (fresh frozen and FFPE tissues) and germline (tumor-free tissue or peripheral blood) samples were collected. Libraries were prepared from 100 to 500 ng of genomic DNA and generated using a SureSelect custom kit (Agilent Technologies), followed by massively parallel sequencing of enriched exon fragments on a HiSeq 2500 with 125-base pair paired-end mode, as previously described.[13,15] Following the manufacturers' protocols,

libraries were prepared using a SureSelect Low Input Automated Target Enrichment System (Agilent Technologies). The mean sequencing coverage across the targeted loci was 277.0×, with 96.8% achieving coverage >20×. For WGS, libraries were prepared from 300 ng of genomic DNA and generated using the TruSeq Nano DNA Library Preparation kit (Illumina) according to the manufacturers' instructions. The mean coverage of WGS was 52.9× in tumor samples and 36.1× in control samples. WES and WGS sequencing statistics are summarized in Table S2. Mutations were called using the in-house pipeline Genomon2 (version 2.5.2.) and EBCall, as previously described.[13] Validation of mutations identified by WES were performed by amplicon-based deep sequencing and targeted deep sequencing, as previously described.[16] The overall validation rate was 92.1% for fresh samples (35/38 mutations) and 91.4% for FFPE samples (127/139 mutations). Validation of mutations identified by WGS were performed by amplicon-based deep sequencing, TS and WES, as previously described.[16] The overall validation rate was 95.4% (267/280 mutations).

Detection of structural variations was performed by Genomon2. Briefly, Genomon2 uses information from chimeric reads (containing breakpoints) and discordant read pairs. For each candidate structural variation, it realigns reads to the assembled contig sequence containing the structural variation breakpoint (variant sequence). Fisher's exact test was performed to compare the proportion of read pairs aligned to variant sequences relative to reference sequences in tumor vs matched normal samples. Putative structural variations were manually curated and further filtered by removing those with (a) Fisher's exact P-value >.01; (b) <4 supporting reads in tumor samples; (c) a VAF in tumor samples <0.1; (d) a VAF in matched normal samples ≥0.02 or (e) length between breakpoints <1000 bp. Identified structural variations were confirmed by PCR and/or Sanger sequencing, in which 24 of 26 (92.3%) variations were validated.

Significantly mutated genes or driver genes, were investigated by analyzing WES data based on MutSigCV (https://www.genepattern.org/modules/docs/MutSigCV) and dNdSCV (https://github.com/im3sanger/dndscv) with their default setting.

Copy number alterations (CANs) were evaluated from WES/targeted deep sequencing data using our in-house pipeline, "CNACS."[16] GISTIC 2.0 (https://www.genepattern.org/modules/docs/GISTIC_2.0) was used to calculate significant CN gains and losses. Amplification and deletions were annotated if copy number of gene of interest is 2 or −2 in the all_thresholded.by_genes.txt file obtained from GISTIC 2.0 analysis, respectively. CNAs in WGS were analyzed by Patchwork (https://patchwork.r-forge.r-project.org/). Mutations, SVs and CNAs detected in WGS were integrated into circos plot (http://circos.ca/). Analysis on chromothripsis were done by sv_tools (https://github.com/PapenfussLab/sv_tools), ShatterSeek (https://github.com/parklab/ShatterSeek) and CTLPscanner (http://cailab.labshare.cn/CTLPScanner/about.php). On the analysis of multiregional/time-point samples, phylogenetic trees were illustrated by MEGAX (https://www.megasoftware.net/). Clonal compositions were analyzed using PyClone (v.0.13.0) (https://github.com/RothLab/pyclone) as previously described.[16]
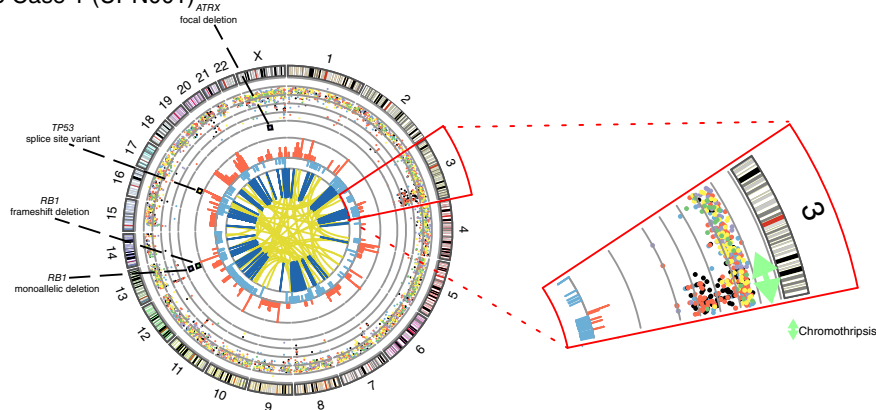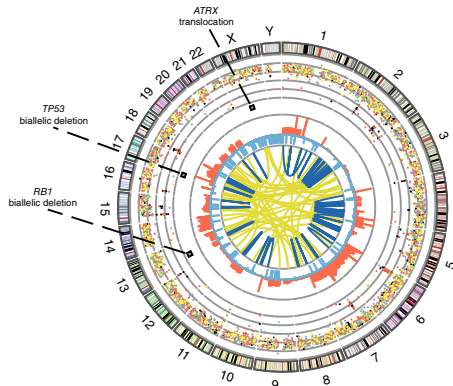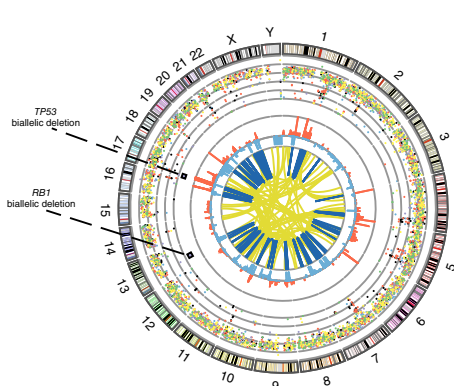
FIGURE 1 Whole genome sequencing of MFS. Five MFS cases were evaluated by WGS, and the circos plots are shown. The types and status of the mutations/copy number alterations/SVs/chromothripsis are shown by the indicated colors [Color figure can be viewed at wileyonlinelibrary.com]
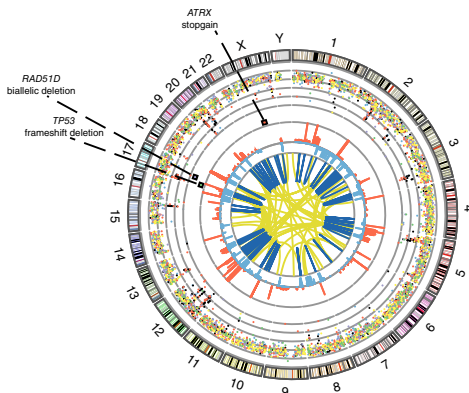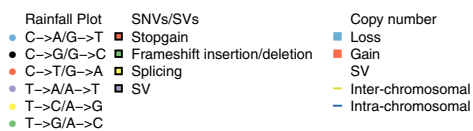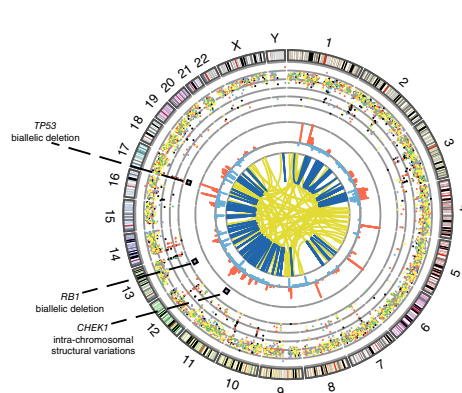
Mutational signatures are analyzed by using whole genome sequencing data. We determined the contribution of known mutational processes reported by Alexandrov et al[17] using the SigProfiler (https://github.com/AlexandrovLab/SigProfilerExtractor). Kataegis is defined by the significant accumulation of the number of mutations, of which adjusted P-value of the frequency of the mutations in 10 kb per 10 Mb calculated based on the Poisson distribution are 10^{-6} or less. Mutational signatures in the kataegis, defined by q-value is 10^{-6}

or less, were calculated by R package deconstructSigs (https://github.com/raerose01/deconstructSigs).

Telomere lengths (TLs) were calculated using TelSeq software (https://github.com/zd1/telseq) from WES data, which was validated for the use on the WES data in the original article. The relative TL ratio was defined as tumor telomere length/normal telomere length (tTL/nTL), that is, the tTL divided by the nTL, corresponding to the pair-matched TL ratio information.
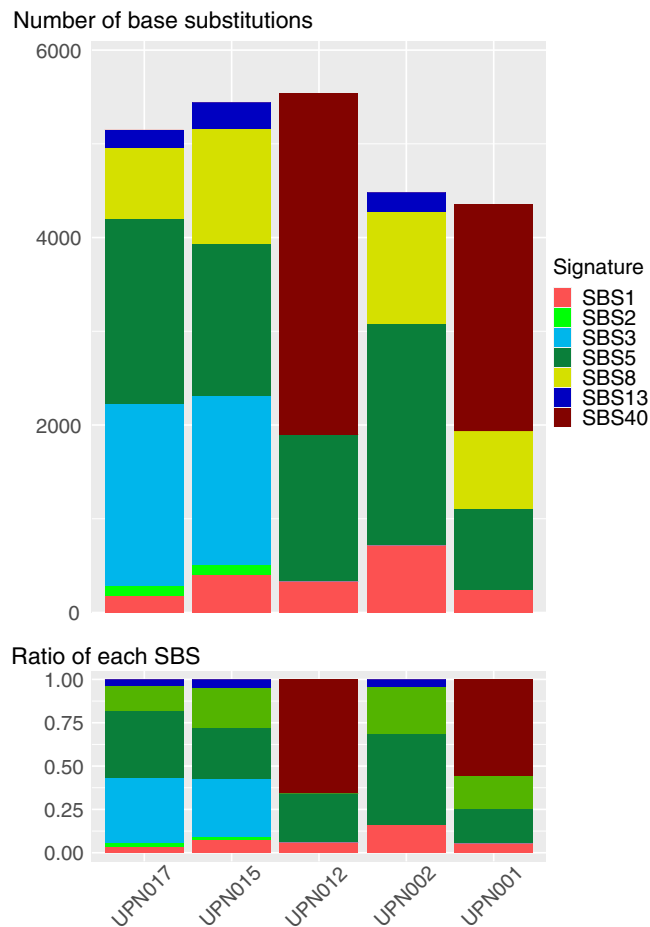
Number of base substitutions

Signature
- SBS1
- SBS2
- SBS3
- SBS5
- SBS8
- SBS13
- SBS40

Ratio of each SBS

FIGURE 2 Mutational signatures of MFS analyzed by WGS. Upper panel shows the number of single base substitutions (SBS) detected in each sample, and the lower panel shows the ratio of the contribution of each SBS [Color figure can be viewed at wileyonlinelibrary.com]

2.3 | Computational analysis

Statistical analyses were performed using R (http://www.R-project.org). Multiple significance testing was adjusted according to the method described by Hochberg and Benjamini.[18] The methods used for the statistical analyses are described in detail in Section 3.

3 | RESULTS

3.1 | Whole-genome sequencing identified a median of 495 structural variations

Five MFS cases were evaluated by whole-genome sequencing (WGS) (Figure 1). All tumors were obtained from the primary site with a mean of 52.9× sequencing depth, by which 96.4% of coding regions were analyzed with a depth >20× on average. A total of 26 716 somatic mutations, including 24 974 single nucleotide variations (SNVs) and 1742 insertion-deletions (indels), were detected with a median of 5149 (1.6/Mb) SNVs and 328 (0.1/Mb) indels per case.

According to an NMF-based decomposition, "clock-like" signatures, namely SBS1, 5 and 40, were predominant, explaining 57.9% of all SNVs. In two cases (ID UPN015 and UPN017; Figure 2), a substantial fraction of SNVs were assigned to SBS3, which is implicated in defective homologous recombination-based DNA damage repair, typically caused by defective BRCA1 or BRCA2.[19] While none of these two cases carried pathogenic somatic/germline variants in *BRCA1* or *BRCA2*, we identified bi-allelic *RAD51D* deletion (UPN015) and *CHEK1*-involving structural variations (SVs) (UPN017),[20] which might have contributed to increased SBS3 mutations in these two cases (Figure 1). APOBEC-related signatures (SBS2/13) were detected in three cases (Figure 2).

In total, we identified 2298 somatic SVs (median: 495 per case), consisting of 434 deletions, 662 inversions, 284 tandem duplications and 918 translocations (Figure 1). Recurrent SVs most frequently affected the *TP53* (n = 4) and *RB1* loci (n = 3) (Figure S2A). In particular, SVs with and without concomitant SNV accounted for the biallelic alteration of *TP53* in three cases carrying intrachromosomal (n = 2) and/or interchromosomal (n = 1) deletions, while it was explained by a combination of a SNV plus an indel in the remaining two cases. Notably, chromothripsis was present in all five samples, with the number of affected chromosomes per tumor ranging from 5 to 10 with a median of 7 (Figure S2B), where chromosomes 2 and 17 were most commonly affected (n = 4, respectively), followed by chromosomes 3, 7 and 13 (n = 3, respectively). Chromothripsis was often accompanied with local hypermutation, so called "kataegis" (Figure 1). Indeed, mutation signature analysis of mutations within the kataegis showed a predominance of APOBEC-related signatures 13 and 2 (38% and 10.0%, respectively), pointing to central role of APOBEC-mediated local hypermutation within the chromothripsis regions.[21]

3.2 | The landscape of genetic alterations in MFS analyzed by WES

Next, we conducted WES of 44 paired tumor and normal samples. All tumors were obtained from the primary site with a mean of 100.3× sequencing depth, by which 90.6% of coding regions were analyzed with a depth >20× on average. In addition, by integrating WES data from 17 MFS samples from the TCGA database[9] and 41 from a previous report,[7] we investigated a total of 102 MFS samples. We detected a total of 7330 somatic mutations with a mean of 50 mutations per case, consisting of 2027 synonymous, 4476 missense, 286 nonsense, 2 stop-loss and 113 splice site SNVs as well as 356 frameshift indels and 70 in-frame indels (Table S3). Driver genes significantly mutated or positively selected in MFS were investigated using MutSigCV and dNdSCV with a *P*-value <.01 (Tables S4 and S5). Besides genes previously known as driver genes in MFS[7-9] such as *TP53* (25/102, 24.5%), *RB1* (23/102, 22.5%), *ATRX* (15/102, 14.7%), *NF1* (9/102, 8.9%) and *TET2* (5/102, 4.9%), we also identified several novel candidates for driver genes including *MUC17* (25/102, 24.5%), *COL6A3* (6/102, 5.9%), *NLRP4* (6/102, 5.9%), *SLC12A5* (6/102, 5.9%), *VCAN* (6/102, 5.9%), *WDR87* (6/102, 5.9%) and *ZNF680* (5/102, 4.9%), each being

mutated in at least five cases and with P-value <.01 in dNdSCV or MutSigCV.

Next, WES data were investigated for CNAs. Using GISTIC 2.0, we identified significant focal amplifications (q-value <0.01) and copy number losses (homozygous and heterozygous deletions) (q-value <0.25) at 35 loci (13 amplifications and 22 copy number losses), including known oncogenes or oncogenic lesions (*DRG2*, *COPS3*, *YAP1*, *JUN*, *AXL*, *SETDB1*, *TFDP1*, 1q21.3 and *PRKD1*),[9,22-30] and tumor suppressors (*TP53*, *CDKN2A*, *CDKN2B*, *RB1*, *HDLBP*, *FANCA*, *AKT3*, *SENP6*, *FH*, *BRD7*, *SNTG2*, *C16orf78* and *MYT1L*)[9,31-38] (Figure 3A). Focal amplifications of *CD274* encoding PD-L1 were identified in four cases (3.9%).

Combining SNV and CNA data, we identified genes recurrently affected by mutations and CNAs that have not been reported previously in MFS. For example, *FLG* were recurrently affected in 24 cases (23.5%) by SNVs (n = 12) (11.8%, P-value and q-value by dNdSCV were .036 and 1, respectively) and amplifications (n = 14) (13.7%, q-value by GISTIC 2.0 was >0.2). *FLG* encodes filaggrin, an intermediate filament-associated protein that aggregates keratin intermediate filaments in mammalian epidermis. While germline mutations leading to loss of FLG function are known to be strong genetic risk factors for allergic diseases, such as atopic dermatitis,[39] oncogenic function of filaggrin has not yet been previously reported. Alterations in *ZNF780A* were also recurrently detected (23 cases, 22.5%), including mutations in nine cases (8.8%, P-value and q-value by dNdSCV were .17 and 1, respectively), amplifications in 11 patients (10.8%, q-value by GISTIC 2.0 was 1.7×10^{-4}) and tandem duplications in four tumors (3.9%).

3.3 | Detailed analysis on genetic alterations in MFS (n = 185) identified mutually exclusive alterations in *CDKN2A/B* and *HDLBP*
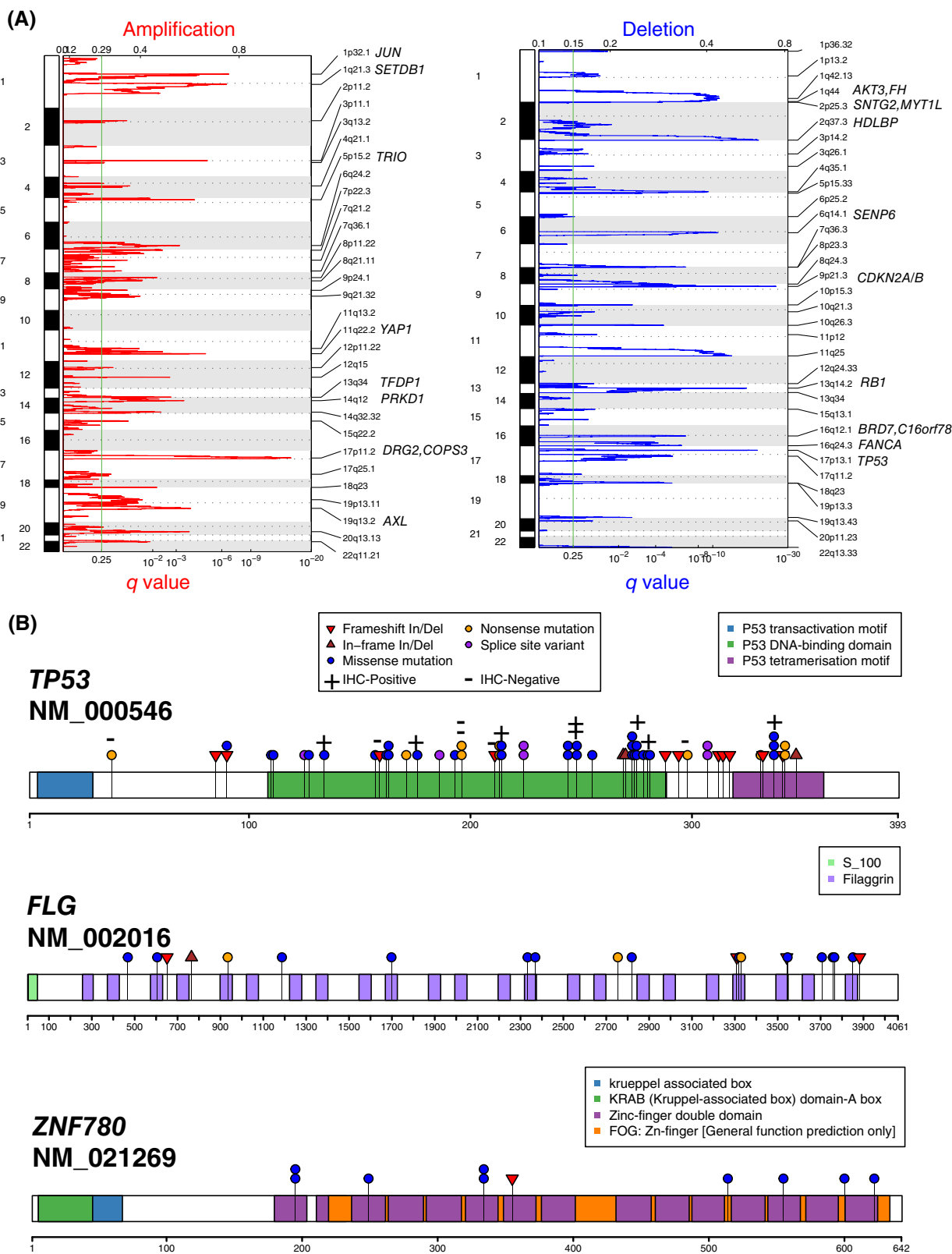
Next, to confirm the findings on WES and further interrogate additional driver alterations involved in MFS pathogenesis, we analyzed 69 MFS cases, including the 44 cases from our WES discovery cohort, by TS of coding and promoter regions of 173 selected genes, including those identified by WES and those identified by a review of the relevant literature.[6,8,9,23,40-42] Intronic regions of driver genes (such as *TP53*, *RB1* and *ATRX*) and a copy number backbone were also integrated to sensitively detect SVs and CNAs. The mean sequencing depth across the targeted loci was 277×, which cover 96.8% of the target regions with >20× depth. Using this approach, we identified 549 nonsilent somatic mutations in 141 genes with a median of six SNVs per tumor. In 43 cases analyzed by both WES and TS, TS detected an additional 141 mutations, validated 80.2% (89/111) of the mutations detected by WES (Table S6). Combining 17 MFS cases from TCGA database[9] and 99 from previous report,[7] we analyzed a total of 185 MFS cases. In accordance with the results from WES, *FLG* and *ZNF780A* were shown to be recurrently mutated (22.8% and 20.5%, respectively) (Figure 3B). The incidence and distribution of driver mutations and CNAs are presented in Figure 4. Although

infrequent, actionable hotspot mutations were identified in *KRAS*, *BRAF* and *PIK3CA* (Figure S3).

For more sensitive detection of *TP53* mutations, 52 tumor samples were further analyzed by IHC for TP53 protein expression using FFPE samples. Immunostaining was negative in 30 cases, the majority of which harbored nonsense/frameshift mutations (n = 7), biallelic deletions (n = 8) or intra/interchromosomal SVs (n = 2). By contrast, 22 cases (42.3%) showed strong staining of TP53 in IHC suggestive of expression of mutant TP53. In fact, 10 (45%) of 22 cases had somatic *TP53* mutations (Figures 3B and 4), including missense mutations (n = 9) cases and one frameshift deletion (NM_000546: p.S314fs), for which the stabilized TP53 is expected on the basis of the registered data in the International Agency for Research on Cancer (IARC) TP53 Mutation Database (http://p53.iarc.fr/). In wild-type state, p53 protein is rapidly degraded by ubiquitination, which results in negative/heterogeneous staining on IHC.[43,44] No genomic alterations in *TP53* were found in 12 cases despite strong TP53 immunostaining in IHC, in which therefore activated, rather than inactivated, TP53 functions are implicated. In general, *TP53* alterations were frequently biallelic events (89/96, 92.7%) most often resulting from a combination of a SNV plus a CNA (n = 54), followed by biallelic deletions (n = 33). As expected, *TP53* alterations were almost mutually exclusive with *MDM2* amplifications (P-value = .020, Fisher's exact test).

We also identified recurrent mutations in regulators of the telomeres in 51 cases (27.6%), which included *ATRX*, *SP100*, *DAXX* and *RBL2* (Figure S4). ATRX cooperates functionally with DAXX, whose mutations are associated with altered telomeres.[45,46] While genetic *DAXX* alterations have not yet been reported in MFSs,[7] we identified two cases with mutations and seven cases with copy number alterations. Deletion of *RBL2* showed a significant positive correlation (P-value: .016, by unequal variances t-test) with relative telomere length, which was evaluated by the ratio of tumor telomere length to normal telomere length and calculated by TelSeq (Figure S5). RBL2, which is also known as Rb-related p130 protein, is reported to suppress telomerase-independent telomere lengthening[47] and, in LMS, deletions of *RBL2* were reported to be correlated with alternative lengthening of telomeres (ALT) activity.[6] These data indicated that frequent genetic alterations in genes of telomere maintenance may accelerate the chromosomal instability in MFS.

Genetic alterations in *HDLBP* (24/127 cases, 18.9%, 22 biallelic deletions and 2 missense mutations) were mutually exclusive (P-value = .007, Fisher's exact test) with biallelic deletions or loss of function mutations in *CDKN2A/B* (39/127 case, 30.7%). *HDLBP* encodes Vigilin, which is among the largest RNA-binding proteins known to date and has been implicated in the induction of double-stranded RNA heterochromatin formation. It represents an emerging cancer pathway, particularly in a mouse model of myxofibrosarcoma.[48] Comprehensive genomic analysis of adult soft tissue sarcoma (n = 206, The Cancer Genome Atlas Research Network,[9] Figure 1A) also showed this pattern of mutual exclusivity between biallelic deletion of *CDKN2A/B* and *HDLBP*, suggesting functional redundancy of *CDKN2A* and *HDLBP* or synthetic lethality in between during sarcomagenesis.
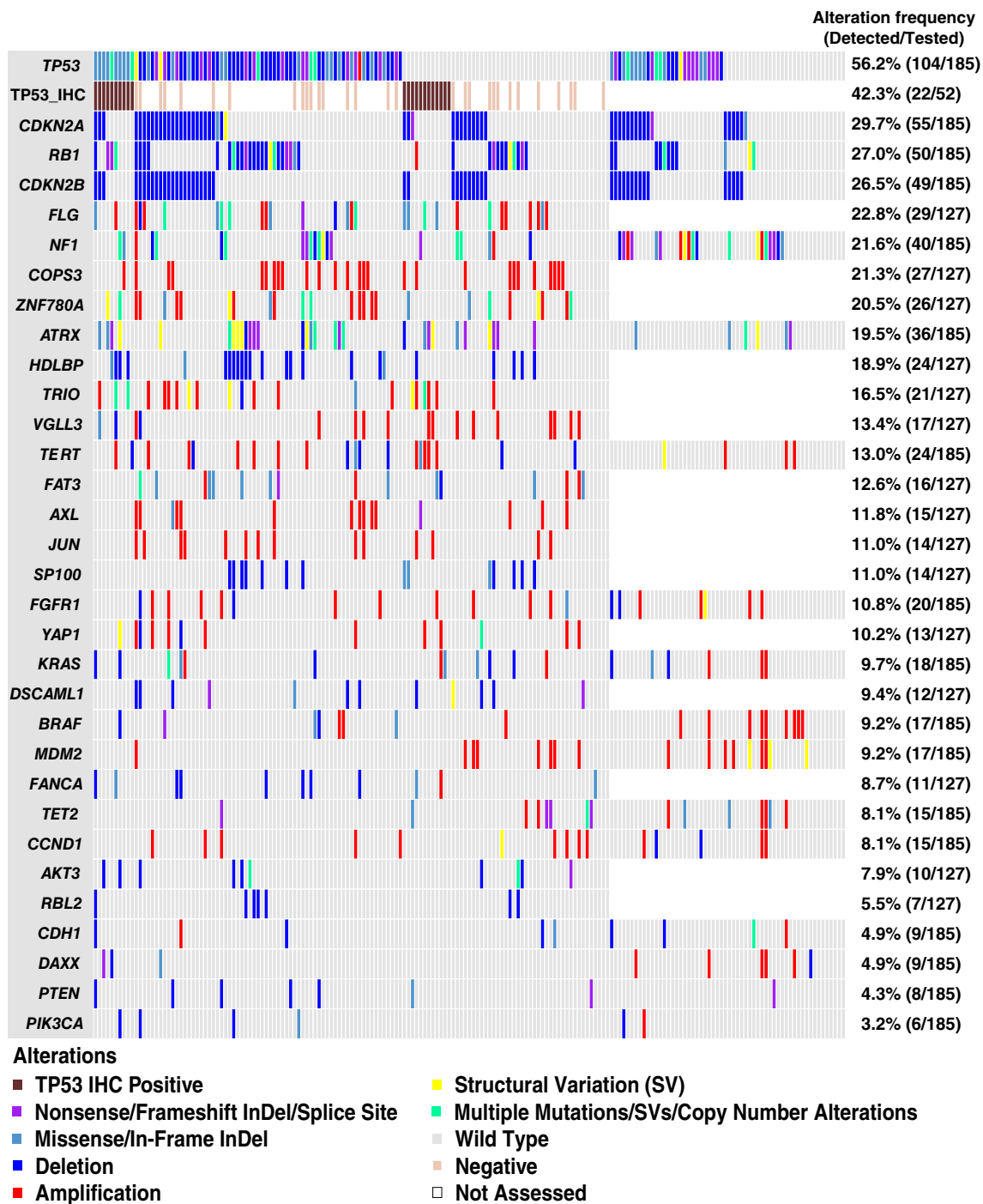
FIGURE 3 Significant copy number alterations, distribution and mutational profile of *TP53*, *FLG* and *ZNF780* genes. (A) Recurrent focal gains (left) and losses (right) analyzed by GISTIC2.0 in WES of 102 cases were plotted. The dashed line indicates the cut-off for significance (*q* = 0.25). For each *q*-value peak, putative gene targets are listed. (B) Lollipop plot showing the distribution and mutation profile in *TP53*, *FLG* and *ZNF780*. The types and status of the somatic alterations are shown by the indicated colors. On the vertical axis the frequency of appearance of each mutation is shown. On the horizontal axis the amino acid position of each mutation is shown [Color figure can be viewed at wileyonlinelibrary.com]

FIGURE 4 Landscape of somatic genetic alterations in MFS. Based on the combined results from our study and previous studies,[7,9] the spectrum of somatic mutations, somatic structural variations, copy number alterations and staining in IHC in MFS are shown. Each column represents an individual case, and each row represents the indicated gene with alteration. The types and status of the somatic alterations are shown by the indicated colors. The frequency of each genetic alteration is shown on the right. IHC, immunohistochemistry; InDel, insertion-deletion [Color figure can be viewed at wileyonlinelibrary.com]

Frequent deletions of genes implicated in DNA double-strand break (DSB) repair have recently reported for LMS.[6] In our cohort, alterations in these DSB repair genes, including *ATR*, *FANCA*, *BRCA1* and *BRCA2*, were found in 59 of 185 cases (31.9%), which were less frequent than reported for LMS (73.5%)[6] (Figure S6). Amplification in *VGLL3* and *MDM2* were significantly enriched in the samples without alterations in DSB repair genes (*P*-value: .047 and .042, respectively, Fisher's exact test). Alterations in *TP53*, *RB1*, *HDLBP*, *FANCA* and *PTEN*, and strong staining in TP53 IHC were significantly enriched in the samples with alterations in DSB repair genes (*P*-value: 3.9×10^{-3}, 2.4×10^{-2}, 7.9×10^{-4}, 4.7×10^{-3}, 6.9×10^{-3} and 4.3×10^{-7}, respectively, Fisher's exact test).

FIGURE 5 Intratumor heterogeneity of MFS with phylogenetic tree. (A) The number of mutations in each sample were plotted and connected by the line with indicated colors. All samples are illustrated in the left panel, and samples with mutation less than 60 are highlighted on the right panel. (B) To further analyze the number of mutation in myxoid component and solid component in each tumor tissue, the number of mutations in each sample were plotted. (C) Phylogenetic trees were illustrated by MEGAX (https://www.megasoftware.net/), and representative genetic alterations are annotated. Representative microscopic images are inserted in each sample [Color figure can be viewed at wileyonlinelibrary.com]
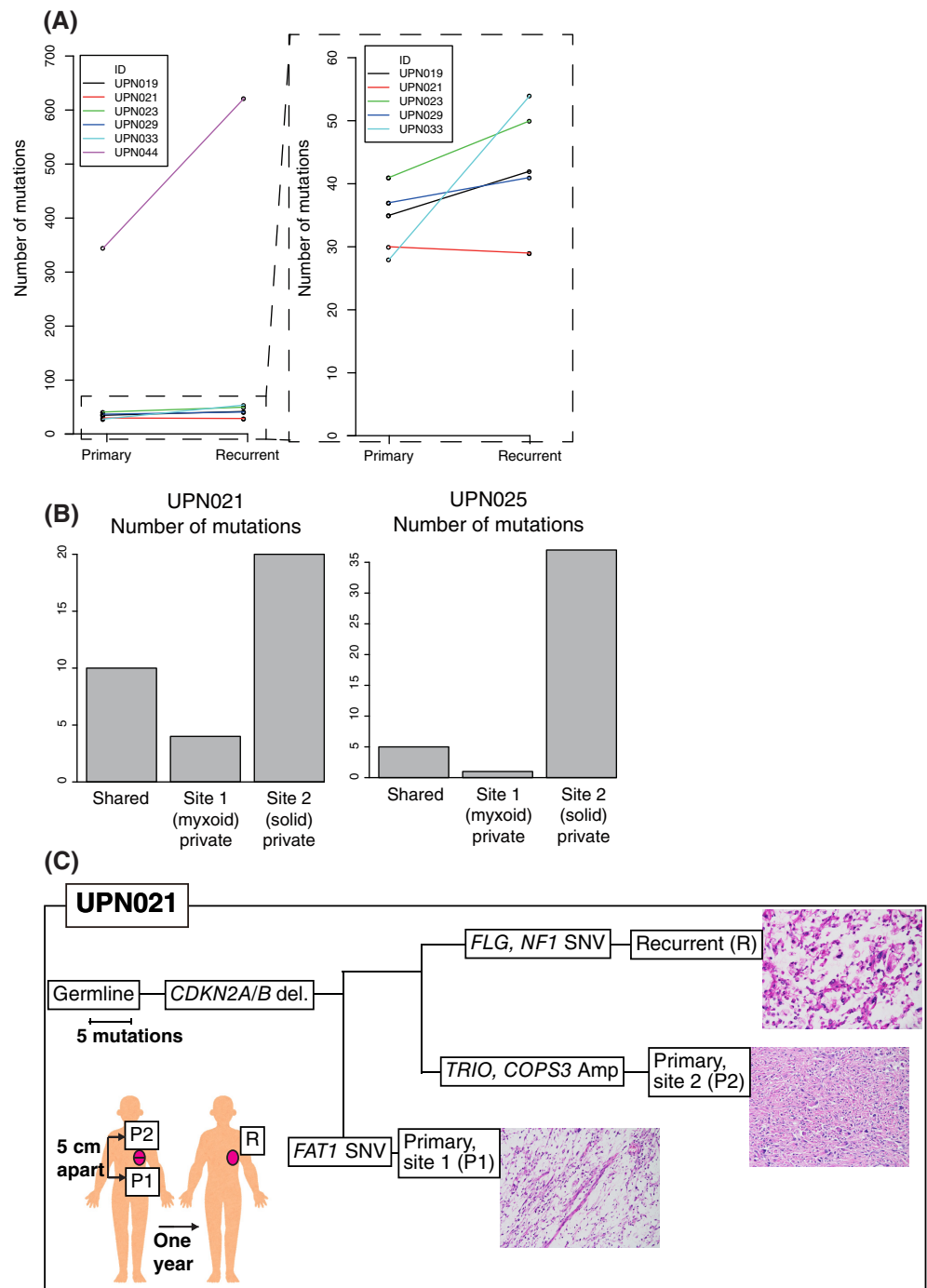
Survival analysis was performed in 63 cases having sufficient clinical data. During a median of 3.2 years of follow-up period, only four patients died, indicating a good prognosis for patients having a resectable, early-stage tumor. Only alterations in *RB1* were marginally associated with poor prognosis (*P*-value = .046). No other genetic alterations or clinical features (surgical margin, histological grade) were significantly associated with patients' prognosis (Figure S7). In addition, we did not identify any significant association between genetic alterations and clinical features (age, gender, tumor location) or tumor characteristics (tumor depth, grade, stage).

3.4 | Whole-exome sequencing with multiregional and/or multi-time-point sampling proved increasing genetic alterations with clinical course of MFS

To elucidate the intratumor heterogeneity and the clonal evolution in MFSs, we performed WES from samples obtained from multiple tumor sites at different time points (Figures 5, S8 and Data S1). For this purpose, we enrolled six patients from whom 16 samples, including seven diagnostic and nine relapse samples, were collected. Macrodissection of thin-sliced unstained FFPE tissues on glass slides was performed to ensure high tumor content. In total 530 (mean: 75.7, median: 35, range:

14-345) and 907 (mean: 100.8, median: 41, range: 19-622) mutations were identified in seven diagnostic and nine relapse samples, respectively. Analysis using a generalized linear mixed model revealed that the number of mutations was significantly larger at relapse (1.2 times on average, *P*-value = .01). This observation holds true, even when excluding those samples from a tumor (UPN044) showing significantly higher number of mutations than the other samples (Figure 5A). Including a patient receiving radiation therapy before disease recurrence (UPN023) (Figure S8), no significant changes in mutational signatures were observed between primary and relapsed tumors. All samples carried at least one alteration in *TP53*, *CDKN2A/B* or *RB1*, all of which were observed in more than 25% of diagnostic samples (Figure 1) and were observed in both diagnostic and relapse samples (Figures 5C and S8). By contrast, alterations in other driver genes were detected in either diagnostic (12/22) or relapse samples (10/22) alone (Figures 5C and S8), suggesting that less frequent driver events lead to substantial clonal diversification including spatial and temporal heterogeneity in MFS tissues.

In two cases multiregional sampling were performed. In each case, two tumor specimens with distinct histological components (myxoid and solid) were analyzed using WES (Figures 5B,C and S8). In each pair of samples, less than 50% of all SNVs and CNAs (SNVs: 20.8% and 45.5%, CNAs: 17.1% and 2.2%) were shared, while the majority of mutations and CNAs were private to each tumor site. In UPN021, both myxoid (site 1) and solid components (site 2) shared a biallelic deletion of *CDKN2A/B*, whereas the myxoid and the solid component harbored private lesions, such as a *FAT1* mutation and amplifications of *TRIO* and *COPS3*, respectively. In UPN025, both myxoid (site 1) and solid components (site 2) harbored an amplification of *TEK*. *TEK* encodes angiopoietin-1 receptor, also known as CD202B (cluster of differentiation 202B) or TIE2, which belongs to the Tie2 family of protein kinase. *TEK* amplification has been reported in breast carcinoma, lung adenocarcinoma, pancreatic adenocarcinoma and anaplastic astrocytoma.[49] In our cohort, only four cases analyzed by WES (4.0%) were shown to harbor *TEK* amplifications. Although no plausible driver genetic alterations were found in myxoid component (site 1), only solid component (site 2) harbored biallelic deletions of *CDKN2A/B*. In both cases, the numbers of mutations detected in solid component (UPN021 site 2: 30 and UPN025 site 2: 42) were higher than those in myxoid component (UPN021 site 1: 14 and UPN025 site 1: 6) (Figure 5B). However, due to the small number of investigated cases, further studies are required to fully capture correlations between genetic alterations and the histological features.

Clonal evolution in MFSs was further analyzed by phylogenetic tree analysis (Figures 5C and S8). Among seven cases, five harbored somatic mutations or CNAs affecting *TP53* or strong staining of p53 in IHC in the "trunk" of the tree, which means the alteration of the *TP53* was the essential driver events in these tumors. Two cases without *TP53* alterations harbored genetic alterations in other driver genes: one case with *TEK* amplification (Figure 5C, UPN025) and the other case with *CDKN2A/B* biallelic deletion (Figure 5C). Analysis by PyClone[50] revealed that base substitutions in *TP53* were clonal events in both cases, which support the notion that alterations in *TP53* are

fundamental events in the tumorigenesis of MFS. Supporting this notion, analysis of cell fraction with base substitution by PyClone or with CNA revealed that in primary MFS samples analyzed by WES (n = 102), almost all alterations in *TP53* (58/60, 96.7%) were clonal events.

4 | DISCUSSION

Here we present a comprehensive genetic study, which to our knowledge included the largest number of MFS cases ever studied. We unravel genetic aberrations commonly observed in MFS and report a remarkable intra-/intertumor heterogeneity in MFS tumor tissue. Genetic aberrations affecting *TP53* were the most frequent alterations and occurred in almost all cases as biallelic events, suggesting that biallelic *TP53* alterations play a crucial role during MFS sarcomagenesis. While recurrent somatic SVs involving the first intron of *TP53* were reported in osteosarcomas,[51] our analysis did not identify similar breakpoints in MFS, although the intronic area of *TP53* was captured by our custom baits. Frequent biallelic involvement of *TP53* alterations resulted from different combinations of SVs, CNAs and SNVs. Based on the recent advances in the understanding of the molecular oncogenesis, many small molecules targeting specific oncogenic proteins, including mutant TP53 inhibitors,[52] are under investigation in clinical trials. It will be of great interest to investigate whether small molecules that restore wild-type p53 functions in *TP53*-mutant cells such as Eprenetapopt (APR-246) and COTI-2 show a similar efficacy in MFS as reported for hematologic malignancies including acute myeloid leukemias.[52]

Another potential target to restore normal p53 function might be an inhibition of overexpressed MDM2 by gene amplification. MDM2 is known to promote degradation of p53 through ubiquitination.[53] *MDM2* amplifications are common in adult soft tissue sarcoma[9] in a mutually exclusive manner with *TP53* mutations, which is a finding that we were able to confirm for MFS. Although amplification of *MDM2* is, as previously described by Ogura et al, a typical marker of the dedifferentiated liposarcoma,[7] it is not a diagnostic finding. In our cohort, all the cases with *MDM2* amplifications arose at the peripheral sites, not the truncal area, and careful pathological review proved that all the cases in our cohort did not harbor liposarcoma-like components. Considering these findings, in concordance with the previous report, we diagnosed these cases as MFS with *MDM2* amplification.[7] Many small molecules targeting MDM2 are currently under evaluation in clinical trials.[54] In addition to mutual exclusiveness with *TP53* aberrations, we identified a significant enrichment of *MDM2* amplifications in samples without alterations in genes involved in DSB repair. Through synthetic lethality, poly (adenosine diphosphate [ADP]-ribose) polymerase (PARP) has antitumor activity in cancer associated with *BRCA* associated gene alterations.[55] Although identification of SBS-3 is known to be difficult on the analysis of mutational signatures,[17] and SBS-3 was identified without concomitant Indel6/8 signatures in our cohort, validation and analysis in even larger MFS cohorts will help to assess the frequency of SBS3-mutations and its usefulness to predict sensitivity to drugs that target defective DSB

repair pathway.[56] In line with this, defective DSB repair pathway as a potentially actionable feature was recently described in leiomyosarcoma (LMS), a sarcoma entity with many genetic commonalities to MFS.[6] LMS and MFS harbor similar genetic alterations such as mutations in genes including *TP53*, *RB1* and *ATRX*, and complex CNAs. However, it should be noted that methylation class prediction revealed substantial epigenetic differences between LMS and MFS, resulting in different class assignments with MFS cases clustering in the undifferentiated sarcoma class.[57] Although mutational landscape and analysis on the tumor evolution revealed that biallelic inactivation of *TP53/RB1* are frequent and fundamental event in both MFS (Figures 4 and 5) and LMS,[6,58] in comparison with MFS genetics, LMS less frequently harbors alterations in *CDKN2A* (8% vs 30% in MFS) and *NF1* (4% vs 22% in MFS), but more commonly affected DSB repair pathway (73.5% vs 32% in MFS). In MFS, various alterations in receptor tyrosine kinase (RTK)-RAS-PI3K cancer pathway (eg, *KRAS*, *BRAF*, *PIK3CA* and *NF1*) were more frequently detected (36.2% vs not described in LMS), which may result in inter- and intratumor heterogeneity of MFS but offer therapeutic windows.

Another disease entity which is known to harbor similar genetic alterations is UPS.[1,9,59] Recent profiling of genetic alterations in UPS revealed frequent alterations in *TP53*, *RB1*, *ATRX* and *CDKN2A* in UPS (65%, 47%, 28% and 25%, respectively),[59] which is similar to the frequency in MFS in our current study. Methylation class prediction cannot differentiate UPS and MFS, both of which was classified as undifferentiated sarcoma class.[57] Considering these findings, until more detailed profiling of genetic/epigenetic/transcriptomic shows clear difference between MFS and UPS, classical histological survey for distinguishing MFS from UPS is mandatory.

In addition to known genetic alterations, we uncovered several recurrent driver genes, which have not previously been identified as driver genes in MFS. These not only included genes that have been found in other cancer and sarcoma entities such as *HDLBP*,[48] but also other genes whose role in carcinogenesis is poorly understood (eg, *ZNF780A*). *HDLBP* encodes vigilin, an RNA-binding protein that has been implicated in the induction of heterochromatin, and was reported as candidate target for chromosomal 2q37.3 deletions in *Sleeping Beauty* transposons screens of sarcoma cell lines. So far, although overexpression of vigilin is reported to be associated with tumor growth of hepatocellular carcinoma,[60] association between sarcomagenesis and vigilin is not yet reported. Detailed analysis of the impact of loss of vigilin and sarcomagenesis is required.

With respect to prognostic impact of genetic alterations in MFS, we were able to confirm an inferior overall survival for patients harboring *RB1* alterations.[7] However, in contrast to previous reports, we did not observe an association between survival and alterations in *TP53* nor *CDKN2A/B*. It should be noted that substantial heterogeneity with respect to presurgical application of chemotherapy with or without hyperthermia and radiotherapy may account for these differences. Even larger cohorts, preferentially enrolled on prospective trials, are warranted to further establish prognostic significance of genetic lesions for individual risk-guidance in MFS.

Taken together, our data provide a comprehensive genetic atlas of MFS sarcomagenesis and suggest at least three avenues for precision medicine guided treatment approaches to further improve patient outcome.

ORCID

Frederik Damm https://orcid.org/0000-0001-5553-1173

REFERENCES

1. WHO. *Classification of Tumours Editorial B: Soft Tissue and Bone Tumours*. Lyon, France: International Agency for Research on Cancer (IARC); 2020.
2. Antonescu C. Round cell sarcomas beyond Ewing: emerging entities. *Histopathology*. 2014;64:26-37.
3. Helman LJ, Meltzer P. Mechanisms of sarcoma development. *Nat Rev Cancer*. 2003;3:685-694.
4. Heinrich MC, Corless CL, Duensing A, et al. PDGFRA activating mutations in gastrointestinal stromal tumors. *Science*. 2003;299:708-710.
5. Hirota S, Isozaki K, Moriyama Y, et al. Gain-of-function mutations of c-kit in human gastrointestinal stromal tumors. *Science*. 1998;279: 577-580.
6. Chudasama P, Mughal SS, Sanders MA, et al. Integrative genomic and transcriptomic analysis of leiomyosarcoma. *Nat Commun*. 2018;9:144.
7. Ogura K, Hosoda F, Arai Y, et al. Integrated genetic and epigenetic analysis of myxofibrosarcoma. *Nat Commun*. 2018;9:2765.
8. Barretina J, Taylor BS, Banerji S, et al. Subtype-specific genomic alterations define new targets for soft-tissue sarcoma therapy. *Nat Genet*. 2010;42:715-721.
9. Cancer Genome Atlas Research Network. Comprehensive and integrated genomic characterization of adult soft tissue sarcomas. *Cell*. 2017;171:950-965.
10. Mentzel T, Calonje E, Wadden C, et al. Clinicopathologic analysis of 75 cases with emphasis on the low-grade variant. *Am J Surg Pathol*. 1996;20:391-405.
11. Shimada S, Ishizawa T, Ishizawa K, Matsumura T, Hasegawa T, Hirose T. The value of MDM2 and CDK4 amplification levels using real-time polymerase chain reaction for the differential diagnosis of liposarcomas and their histologic mimickers. *Hum Pathol*. 2006;37: 1123-1129.
12. Ishibashi H, Suzuki T, Suzuki S, et al. Sex steroid hormone receptors in human thymoma. *J Clin Endocrinol Metab*. 2003;88:2309-2317.
13. Polprasert C, Takeuchi Y, Kakiuchi N, et al. Frequent germline mutations of HAVCR2 in sporadic subcutaneous panniculitis-like T-cell lymphoma. *Blood Adv*. 2019;3:588-595.
14. Hoyer K, Hablesreiter R, Inoue Y, et al. A genetically defined signature of responsiveness to erlotinib in early-stage pancreatic cancer patients: results from the CONKO-005 trial. *EBioMedicine*. 2021;66:103327.
15. Mylonas E, Yoshida K, Frick M, et al. Single-cell analysis based dissection of clonality in myelofibrosis. *Nat Commun*. 2020;11:73.
16. Yokoyama A, Kakiuchi N, Yoshizato T, et al. Age-related remodelling of oesophageal epithelia by mutated cancer drivers. *Nature*. 2019; 565:312-317.
17. Alexandrov LB, Kim J, Haradhvala NJ, et al. The repertoire of mutational signatures in human cancer. *Nature*. 2020;578:94-101.
18. Hochberg Y, Benjamini Y. More powerful procedures for multiple significance testing. *Stat Med*. 1990;9:811-818.
19. Powell SN, Kachnic LA. Roles of BRCA1 and BRCA2 in homologous recombination, DNA replication fidelity and the cellular response to ionizing radiation. *Oncogene*. 2003;22:5784-5791.
20. Radhakrishnan SK, Bebb DG, Lees-Miller SP. Targeting ataxia-telangiectasia mutated deficient malignancies with poly ADP ribose polymerase inhibitors. *Transl Cancer Res*. 2013;2:155-162.
21. Cortes-Ciriano I, Lee JJ, Xi R, et al. Comprehensive analysis of chromothripsis in 2,658 human cancers using whole-genome sequencing. *Nat Genet*. 2020;52:331-341.
22. Yoon NA, Jung SJ, Choi SH, et al. DRG2 supports the growth of primary tumors and metastases of melanoma by enhancing VEGF-A expression. *FEBS J*. 2020;287:2070-2086.
23. Behjati S, Tarpey PS, Haase K, et al. Recurrent mutation of IGF signalling genes and distinct patterns of genomic rearrangement in osteosarcoma. *Nat Commun*. 2017;8:15936.
24. Zhang X, Ren D, Guo L, et al. Thymosin beta 10 is a key regulator of tumorigenesis and metastasis and a novel serum marker in breast cancer. *Breast Cancer Res*. 2017;19:15.
25. Goh JY, Feng M, Wang W, et al. Chromosome 1q21.3 amplification is a trackable biomarker and actionable target for breast cancer recurrence. *Nat Med*. 2017;23:1319-1330.
26. Melchor L, Saucedo-Cuevas LP, Munoz-Repeto I, et al. Comprehensive characterization of the DNA amplification at 13q34 in human breast cancer reveals TFDP1 and CUL4A as likely candidate target genes. *Breast Cancer Res*. 2009;11:R86.
27. Fei Q, Shang K, Zhang J, et al. Histone methyltransferase SETDB1 regulates liver cancer cell growth through methylation of p53. *Nat Commun*. 2015;6:8651.
28. Gay CM, Balaji K, Byers LA. Giving AXL the axe: targeting AXL in human malignancy. *Br J Cancer*. 2017;116:415-423.
29. Mariani O, Brennetot C, Coindre JM, et al. JUN oncogene amplification and overexpression block adipocytic differentiation in highly aggressive sarcomas. *Cancer Cell*. 2007;11:361-374.
30. Helias-Rodzewicz Z, Perot G, Chibon F, et al. YAP1 and VGLL3, encoding two cofactors of TEAD transcription factors, are amplified and overexpressed in a subset of soft tissue sarcomas. *Genes Chromosomes Cancer*. 2010;49:1161-1171.
31. Flynn EK, Kamat A, Lach FP, et al. Comprehensive analysis of pathogenic deletion variants in Fanconi anemia genes. *Hum Mutat*. 2014; 35:1342-1353.
32. Shu XS, Li L, Ji M, et al. FEZF2, a novel 3p14 tumor suppressor gene, represses oncogene EZH2 and MDM2 expression and is frequently methylated in nasopharyngeal carcinoma. *Carcinogenesis*. 2013;34: 1984-1993.
33. Cuppens T, Moisse M, Depreeuw J, et al. Integrated genome analysis of uterine leiomyosarcoma to identify novel driver genes and targetable pathways. *Int J Cancer*. 2018;142:1230-1243.
34. Melhuish TA, Kowalczyk I, Manukyan A, et al. Myt1 and Myt1l transcription factors limit proliferation in GBM cells by repressing YAP1 expression. *Biochim Biophys Acta Gene Regul Mech*. 2018;1861: 983-995.
35. Li J, Lu D, Dou H, et al. Desumoylase SENP6 maintains osteochondroprogenitor homeostasis by suppressing the p53 pathway. *Nat Commun*. 2018;9:143.
36. Yu X, Li Z, Shen J. BRD7: a novel tumor suppressor gene in different cancers. *Am J Transl Res*. 2016;8:742-748.
37. Yang J, Du X, Chen K, et al. Genetic aberrations in soft tissue leiomyosarcoma. *Cancer Lett*. 2009;275:1-8.
38. Liegl-Atzwanger B, Heitzer E, Flicker K, et al. Exploring chromosomal abnormalities and genetic changes in uterine smooth muscle tumors. *Mod Pathol*. 2016;29:1262-1277.
39. Skaaby T, Husemoen LL, Thyssen JP, et al. Filaggrin loss-of-function mutations and incident cancer: a population-based study. *Br J Dermatol*. 2014;171:1407-1414.
40. Kovac M, Blattmann C, Ribi S, et al. Exome sequencing of osteosarcoma reveals mutation signatures reminiscent of BRCA deficiency. *Nat Commun*. 2015;6:8940.
41. Heitzer E, Sunitsch S, Gilg MM, et al. Expanded molecular profiling of myxofibrosarcoma reveals potentially actionable targets. *Mod Pathol*. 2017;30:1698-1709.
42. Cheng J, Demeulemeester J, Wedge DC, et al. Pan-cancer analysis of homozygous deletions in primary tumours uncovers rare tumour suppressors. *Nat Commun*. 2017;8:1221.
43. Kobel M, Ronnett BM, Singh N, Soslow RA, Gilks CB, McCluggage WG. Interpretation of P53 immunohistochemistry in endometrial carcinomas: toward increased reproducibility. *Int J Gynecol Pathol*. 2019;38(Suppl 1): S123-S131.
44. Yemelyanova A, Vang R, Kshirsagar M, et al. Immunohistochemical staining patterns of p53 can serve as a surrogate marker for TP53 mutations in ovarian carcinoma: an immunohistochemical and nucleotide sequencing analysis. *Mod Pathol*. 2011;24:1248-1253.
45. Heaphy CM, de Wilde RF, Jiao Y, et al. Altered telomeres in tumors with ATRX and DAXX mutations. *Science*. 2011;333:425.

46. Jiao Y, Shi C, Edil BH, et al. DAXX/ATRX, MEN1, and mTOR pathway genes are frequently altered in pancreatic neuroendocrine tumors. *Science*. 2011;331:1199-1203.

47. Kong LJ, Meloni AR, Nevins JR. The Rb-related p130 protein controls telomere lengthening through an interaction with a Rad50-interacting protein, RINT-1. *Mol Cell*. 2006;22:63-71.

48. Molyneux SD, Waterhouse PD, Shelton D, et al. Human somatic cell mutagenesis creates genetically tractable sarcomas. *Nat Genet*. 2014; 46:964-972.

49. Consortium APG. AACR project GENIE: powering precision medicine through an international consortium. *Cancer Discov*. 2017;7:818-831.

50. Roth A, Khattra J, Yap D, et al. PyClone: statistical inference of clonal population structure in cancer. *Nat Methods*. 2014;11:396-398.

51. Chen X, Bahrami A, Pappo A, et al. Recurrent somatic structural variations contribute to tumorigenesis in pediatric osteosarcoma. *Cell Rep*. 2014;7:104-112.

52. Sallman DA, DeZern AE, Garcia-Manero G, et al. Eprenetapopt (APR-246) and Azacitidine in TP53-mutant myelodysplastic syndromes. *J Clin Oncol*. 2021;39:1584-1594.

53. Oliner JD, Pietenpol JA, Thiagalingam S, Gyuris J, Kinzler KW, Vogelstein B. Oncoprotein MDM2 conceals the activation domain of tumour suppressor p53. *Nature*. 1993;362:857-860.

54. Wang W, Qin JJ, Rajaei M, et al. Targeting MDM2 for novel molecular therapy: beyond oncology. *Med Res Rev*. 2020;40:856-880.

55. Fong PC, Boss DS, Yap TA, et al. Inhibition of poly(ADP-ribose) polymerase in tumors from BRCA mutation carriers. *N Engl J Med*. 2009; 361:123-134.

56. Davies H, Glodzik D, Morganella S, et al. HRDetect is a predictor of BRCA1 and BRCA2 deficiency based on mutational signatures. *Nat Med*. 2017;23:517-525.

57. Koelsche C, Schrimpf D, Stichel D, et al. Sarcoma classification by DNA methylation profiling. *Nat Commun*. 2021;12:498.

58. Anderson ND, Babichev Y, Fuligni F, et al. Lineage-defined leiomyosarcoma subtypes emerge years before diagnosis and determine patient survival. *Nat Commun*. 2021;12:4496.

59. Steele CD, Tarabichi M, Oukrif D, et al. Undifferentiated sarcomas develop through distinct evolutionary pathways. *Cancer Cell*. 2019; 35:441-456.

60. Yang WL, Wei L, Huang WQ, et al. Vigilin is overexpressed in hepatocellular carcinoma and is required for HCC cell proliferation and tumor growth. *Oncol Rep*. 2014;31:2328-2334.

SUPPORTING INFORMATION

Additional supporting information may be found in the online version of the article at the publisher's website.